Volume 22, No 4 | International Journal of Radiation Research, October 2024

Clinical value of CT imaging features to predict infiltration degree and pathological subtype of ground glass lung adenocarcinoma

X. Gong[1,2] and C. Huang[1*]

[1]*Department of Thoracic Surgery, Nanjing Medical University, The First Affiliated Hospital of Nanjing Medical University, Jiangsu Province Hospital, Nanjing, China*
[2]*Department of Thoracic Surgery, Jiangyin Hospital Affiliated to Nanjing University of Chinese Medicine, Jiangyin Hospital of Traditional Chinese Medicine, Jiangyin, China*

► ***Original article***

***Corresponding author:**
Chenjun Huang,
E-mail:
huangchenjun2022@163.com

Received: March 2024
Final revised: May 2024
Accepted: May 2024

Int. J. Radiat. Res., October 2024; 22(4): 909-918

DOI: 10.61186/ijrr.22.4.909

Keywords: *ground glass nodules, pathological subtype, imaging features, lung adenocarcinoma, degree of infiltration.*

ABSTRACT

Background: To test the value of Computed tomography (CT) features in predicting the infiltration degree and pathological subtype of ground glass lung adenocarcinoma (≤ 3 cm). ***Materials and Methods:*** Data from 412 lung adenocarcinoma patients with mixed ground glass nodules on CT from Jan. 2017 to Dec. 2021 were tested retrospectively. The patients were separated by the infiltrating degree into a minimally invasive adenocarcinoma (MIA) group and an invasive adenocarcinoma (IAC) group. Then the IAC group was subdivided into low-, medium- and high-risk groups by the prognosis differences among subtypes, which were of lepidic, papillary, and micropapillary predominance respectively. ***Results:*** Average diameter of nodules, average CT value, solid component ratio, lobe sign, and burr sign were independent risk factors of IAC. The average diameter of nodules ≥ 12.5 mm, solid component ratio ≥ 20.96%, average CT value ≥ -473.07 HU, positive lobe sign and positive burr sign indicated the nodules were more likely IAC. Average CT value, and solid component ratio were independent risk factors for the high-risk pathological type of lung adenocarcinoma. The average CT value ≥ -242.92 HU and solid component ratio ≥ 69.536% indicated nodules were more likely the high-risk pathological type of lung adenocarcinoma. ***Conclusion:*** CT imaging features improve the diagnostic efficacy of ground glass nodules, and have certain clinical value.

INTRODUCTION

Based on the 2020 Global Cancer Report, lung cancer is still the leading cause of cancer-related deaths, with adenocarcinoma as its major histological subtype [1]. Adenocarcinoma in situ (AIS), minimally invasive adenocarcinoma (MIA), and invasive adenocarcinoma (IAC) are the four subtypes of lung cancer recognized by the World Health Organization (WHO) [2]. In lung cancer with varying degrees of infiltration, the 5-year disease-free survival rate is 100% for AIS and MIA that have been completely resected, but it is only 89% for stage Ia IAC [3, 4]. Adenocarcinomas classified as invasive mucinous adenocarcinomas will no longer be considered pathological subtypes of mutant IACs, but rather histopathological types. As of now, there are five pathological types of IAC: acinir-growing, papillary-growing, solid-growing, and micropapillary-growing [5,6]. Specific types with low recurrence rates include lepidic growing, papillary, and solid types with the highest recurrence rates [7]. Studies have also demonstrated a significant correlation between aggressive clinical characteristics and poor prognosis when there are minimal solid or micropapillary components present..

Anatomical lobectomy is still the standard operation for lung cancer, but with the application of high resolution computed tomography (CT), the detection rate of early lung nodules has gradually increased, and sublobectomy has been more and more widely used in early lung cancer. In a retrospective study 5 to determine the significance of histological subtypes in surgical decision making, recurrent-free survival (RFS) and overall survival (OS) with intraoperative segmentectomy were significantly worse than those with lobal resection. Another retrospective study 3 found that pathological subtypes of lung adenocarcinoma played an important role in lymph node metastasis of small focal lung adenocarcinoma, and the lymph node metastasis rate of lung adenocarcinoma containing solid and micropapillary subtypes was significantly higher than that of other subtypes. The significance of this study is that if the pathological subtypes of lung adenocarcinoma can be predicted before surgery, some patients can receive sublobectomy. And benefit from individualized surgery [8,9]. However, at present, it is difficult to identify the pathological subtypes of lung adenocarcinoma in a timely and accurate

[DOI: 10.61186/ijrr.22.4.909]

manner before or during the operation. Some studies have found that the accuracy of determining the tissue type of adenocarcinoma by preoperative biopsy is not ideal, and the coincidence rate between the diagnosis of adenocarcinoma and postoperative paraffin histopathological specimens is only 58.6%. In addition, it has been reported that intraoperative freeze pathology has high specificity for the diagnosis of micropapillary subtypes in invasive adenocarcinoma, but its sensitivity is poor and it is difficult to predict the dominant pattern on the basis of frozen sections. Therefore, a better understanding of the relationship between solid and micropapillary subtypes in lung adenocarcinoma and clinical imaging and pathology is conducive to improving the differentiation of solid and micropapillary pathological subtypes before surgery, which has a certain effect on the selection of appropriate surgical methods and the scope of lymph node dissection during surgery, and the reduction of tumor residue in patients. In addition, it is also conducive to developing further postoperative treatment strategies for patients with different pathological subtypes, and has a positive effect on improving the postoperative survival rate of patients.

Choosing the right surgical method and treatment options requires a thorough assessment of the degree of nodule infiltration and the pathological subtype before surgery. Computed tomography (CT) is an important method for diagnosis of lung cancer. The novel feature of this study is the value of CT features in predicting the degree of invasion and pathological subtypes of ground-glass lung adenocarcinoma (≤ 3cm). CT image features can improve the diagnostic efficiency of ground-glass nodules and have certain clinical value. In this study, the computed tomography (CT) characteristics were analyzed to investigate the correlation between infiltration degrees and pathological subtypes of pulmonary nodules, with the aim of identifying significant imaging features that can enhance diagnostic accuracy.

MATERIALS AND METHODS

Subjects

Retrospective analysis of medical records of 412 lung adenocarcinoma patients diagnosed in our hospital in the period between Jan. 2017 and Dec. 2021 revealed mixed-density ground-glass pulmonary nodules. The name of the ethical committee approving the study is [Jiangyin Hospital of Traditional Chinese Medicine]. The ethical approval registration number is [EC202201] and the date of registration is [2022.01.12]. Inclusion criteria were: (1) complete and correct relevant clinical data and pathological results; (2) solitary nodules in diameter ≤ 3 cm, no evidence of lymph node or distant metastasis; (3) no reception of anti-tumor treatment in the past; (4) complete preoperative chest CT imaging data in our hospital. Exclusion criteria were (1) multiple mGGN on CT images; (2) lymph node metastasis or distant metastasis; (3) lack of CT imaging data from our hospital before surgery; (4) reception of anti-tumor treatment before surgery. Approval was offered by the Ethics Committee of our hospital, and informed consents were provided by all patients.

CT method

CT scanning methods: All patients underwent chest CT scanning in the imaging department of our hospital within one month before surgery (instrument parameters: Siemens 64-slice spiral CT, tube voltage 120 kV, tube current 120 mA, matrix 512 × 512, layer thickness 1.0 mm, layer spacing 0.6 mm, pitch 1.0, reconstructed layer thickness 1.0 mm). Scanning process: The patient was lying flat on the CT examination bed with his hands raised above his head. The scanning range was from the neck base to the adrenal gland, including the armpits and thorax on both sides. After deep inspiration, the patient held his breath and scanned continuously from top to bottom. CT image interpretation: two senior physicians jointly analyze the records. When there is no consensus on the view, the department will consult to determine the characteristics of CT signs.

Image analysis

The clinical information of the patients was hidden. The images were read, analyzed and diagnosed by two radiologists who had been specializing in chest imaging analysis and diagnosis for over 5 years. The CT image characteristics of the lesions were recorded by the radiologists. Any disagreement between them was discussed with another senior physician, and then the final judgment was made. A part of the images were analyzed using a medical image processing system (Hangzhou Shenrui Bolian Technology Co., Ltd.). There was a CT cutoff of -250 Hu for solid components, and an upper CT limit was set by default. This limit was set at 100 Hu if it was too large, and any part exceeding that was considered calcification.

Evaluation contents and standards

Relevant parameters were determined through extensive literature review. The parameters tested included age, gender, smoking history, respiratory symptoms, family history of lung cancer, CEA levels, nodule characteristics, and various signs and measurements on CT scans. Based on the maximum cross-sectional area, longest diameter, and vertical diameter of the nodules, we calculated the average nodule diameter. Average CT value, nodule volume, solid component volume, and solid component ratio: CT data were imported into the medical image

[DOI: 10.61186/ijrr.22.4.909]

processing system for automatic analysis and calculation. Solid component ratio was defined as solid component volume/nodule volume * 100%. The image processing system was utilized to stain nodules and solid components individually, followed by an assessment of the shape (round-like, irregular), quantity (single, multiple), distribution (concentrated, scattered), and location (center, eccentric) of said solid components (figure 1). Nodule boundary and solid component boundary: The boundaries of nodules or solid components were compared before and after staining. Clear boundaries are defined as those that are consistent before and after staining; unclear boundaries are defined as those that are not consistent before and after staining (figure 2).

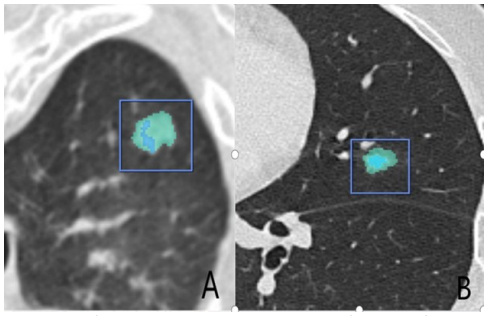

Figure 1. A single, eccentric, concentrated, irregular; **B** single, center, concentrated, round-like.

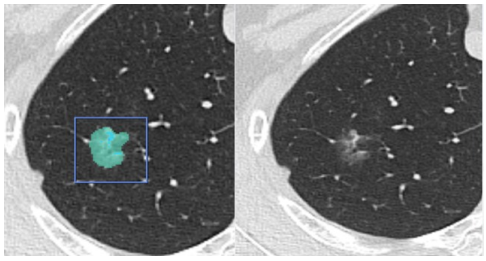

Figure 2. Nodule with unclear boundary, clear solid component.

Pathological analysis

All excised tumor tissue specimens were fixed in 10% neutral formalin solution for 12-48 h after in vitro (approval number: Beijing Drug Administration (quasi) word 2011 No. 1400617, China), and then sampling, paraffin embedding (Shaoxing Zhende Medical Dressing Co., LTD., China), section, hematoxylin/eosin routine staining (Hangzhou Wanbon Tiancheng Pharmaceutical Co., LTD., China), light microscope observation, and finally according to the 2015 IASLC/ATS/ERS international classification provisions. Each histological subtype was recorded in 5% increments in a double-blind review by two senior pathologists. Diagnosis was made by pathologists with over 15 years of working experience, according to the 2015 WHO Classification Criteria for Lung Cancer.

Statistical analysis

Data were statistically analyzed on R Foundation for Statistical Computing 4.3.2 (Vienna, Austria). Measured data in normal distribution were statistically expressed as mean ± standard deviation, and compared via t-test and one-way analysis of variance between and among groups respectively. Data not in normal distribution were described as median [P25, P75] and compared between groups via rank sum test. Counting data were described as the number of cases (%), and compared between groups via Chi-square test or by Fisher's exact probability test. Variables with significant differences were screened out, and then sent to logistic regression analysis. Based on the analysis results, a receiver's operating characteristic (ROC) curve was drawn and the optimal critical value was determined. All statistical tests were two-sided. $P < 0.05$ indicates significance.

RESULTS

Clinical data

The total number of patients included in the study was 412, divided into two groups according to the degree of infiltration: MIA group (151) and IAC group (261). There were significant differences between the two groups in gender and age (table 1).

Analysis of imaging features in MIA group and IAC group

Both groups had significantly different average nodule diameters and CT values, as well as nodule volumes, solid component volumes, solid ratios, solid component boundaries, and vascular convergence signs (table 2).

Correlation analysis between image features and infiltration degree

Univariate analysis revealed that gender, age, average nodule diameter, average CT value, nodule volume, solid component volume, solid component ratio, solid component boundary, vascular convergence sign, lobe sign, and burr sign were statistically significant ($P < 0.05$) and were subsequently included in a multifactor logistic regression model. The results indicated that average nodule diameter, average CT value, solid component ratio, lobe sign, and burr sign were identified as crucial factors for distinguishing between the two groups (table 3). The ROC curve analysis revealed the optimal cutoff of average nodule diameter was 12.5 mm, with AUC of 0.859, sensitivity of 73.6% and specificity of 89.4%, which were 20.96%, 0.725, 87.0% and 53.0% for the solid component ratio respectively, and were -473.07 HU, 0.659, 61.7% and 72.8% for average CT value respectively, The AUC, sensitivity and specificity of lobe sign were 0.648, 39.5% and 90.1% respectively, and were 0.711, 50.2% and 92.1% for burr sign respectively. The combined prediction effect is the best, with AUC of

[DOI: 10.61186/ijrr.22.4.909]

0.928, sensitivity of 82.8% and specificity of 90.7% (table 4, figure 3).

Data analysis of different pathological subtypes

The IAC group was subdivided into low-, medium-, and high-risk groups (lepidic, papillary or acinar, and micropapillary & solid predominant respectively) according to the prognostic differences among pathological subtypes. There were 89, 125 and 47 cases in the three groups respectively. The three groups showed significant differences in gender, respiratory symptoms, nodule location, average nodule diameter, average CT value, nodule volume, nodule boundary, burr sign, air bronchogram, and the volume, ratio, location and boundary of solid components (table 5).

Correlation analysis between imaging features and pathological subtypes

After the low- and medium-risk groups were combined, the single-factor logistic regression demonstrated the average nodule diameter, average CT value, nodule volume and boundary, solid component volume and ratio, pleural indentation sign, and burr sign may be the risk factors in the high -risk group (table 6).

The average nodule diameter, average CT value, nodule volume and boundary, solid component volume and ratio, pleural indentation sign, and burr sign were significant in single-factor analysis ($P < 0.05$), and were involved in the multifactor logistic regression. Results showed the average CT value and solid component ratio were independent risk factors in the high-risk group (table 7). ROC curve analysis determined the optimal cutoff of average CT value was -242.92 HU, with AUC of 0.815, sensitivity of 66.0% and specificity of 87.4%, which were 69.536%, 0.861, 76.6% and 88.8% for the solid component ratio respectively. The combined prediction effect is the best, with AUC of 0.891, sensitivity of 74.5% and specificity of 87.9% (table 8, figure 4).

Typical cases

1. The patient is female 72 years old. Mixed density ground glass nodules of left upper lobe, burr sign, lobed sign. The average CT value was -36.0HU, the average diameter was 13.5mm, and the firmness accounted for 91.4%. Pathology showed infiltrating adenocarcinoma, mainly micropapillary subtype (figure 5).

2. The patient is female 62 years old. Mixed density ground glass nodules in upper lobe of right lung, burr sign, lobed sign. The average CT value was -74.3.0HU, the average diameter was 15mm, and the proportion of firmness was 84.8 %. Pathology showed infiltrating adenocarcinoma, mainly micropapillary subtype (figure 6).

Table 1. Clinical data of MIA group and IAC group.

Variables	MIA (n = 151)	IAC (n = 261)	Z/χ^2	*P*
Gender, n (%)			4.546	0.033
Female	105 (69.5)	154 (59)		
Male	46 (30.5)	107 (41)		
Age, [y, M(Q1,Q3)]	58.00 (52.00, 66.00)	62.00 (57.00, 68.00)	-3.863	< 0.001
History of smoking, n (%)			0.207	0.649
No	132 (87.4)	224 (85.8)		
Yes	19 (12.6)	37 (14.2)		
Respiratory symptoms, n (%)			0.137	0.712
No	131 (86.8)	223 (85.4)		
Yes	20 (13.2)	38 (14.6)		
Family history of lung cancer, n (%)			1.571	0.210
No	146 (96.7)	245 (93.9)		
Yes	5 (3.3)	16 (6.1)		
Carcinoembryonic antigen CEA, n (%)			0.622	0.430
Normal	145 (96)	246 (94.3)		
Increase	6 (4)	15 (5.7)		

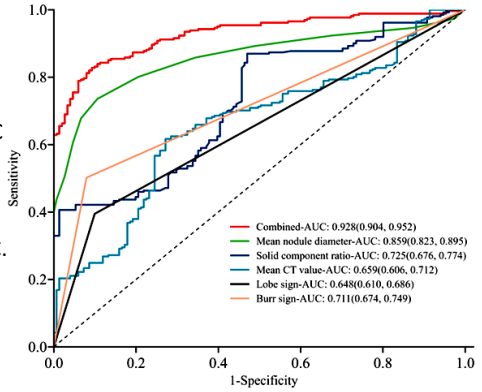

Figure 3. ROC curve of imaging features for predicting IAC.

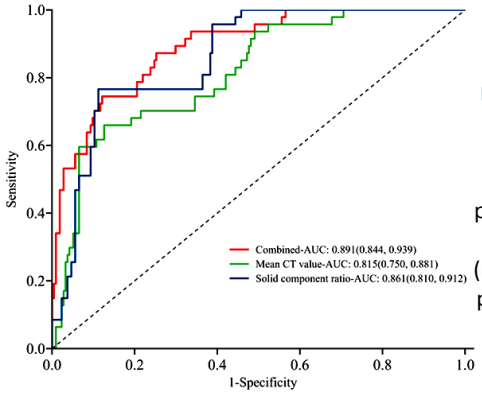

Figure 4. ROC curve of imaging features in predicting high -risk group (micropapillary predominant).

[DOI: 10.61186/ijrr.22.4.909]

Table 2. Imaging features in MIA group and IAC group.

Variables	MIA (n = 151)	IAC (n = 261)	Z/χ^2	P
Location of nodule, n (%)			2.327	0.312
Inner zone	24 (15.9)	35 (13.4)		
Middle zone	26 (17.2)	61 (23.4)		
Outer zone	101 (66.9)	165 (63.2)		
Mean nodule diameter, [mm,M (Q1,Q3)]	9.00 (8.00, 11.00)	16.00 (12.00, 21.00)	-12.168	< 0.001
Mean CT value, [HU,M(Q1,Q3)]	-549.20 (-602.04, -449.95)	-427.60 (-563.00, -261.91)	-5.380	< 0.001
Nodule volume, [mm^3,M(Q1,Q3)]	766.35 (481.68, 1357.55)	1811.16 (846.44, 2850.24)	-8.505	< 0.001
Nodule boundary, n (%)			0.339	0.560
Unclear	36 (23.8)	69 (26.4)		
Clear	115 (76.2)	192 (73.6)		
Solid component volume, [mm^3,M (Q1,Q3)]	255.66 (28.96, 690.13)	533.78 (135.36, 1217.00)	-5.498	< 0.001
Solid component ratio (%), M (Q1,Q3)	19.83 (14.70, 29.89)	29.44 (23.49, 68.20)	-7.611	< 0.001
Solid component shape, n (%)			1.834	0.176
Irregular	145 (96)	242 (92.7)		
Round-like	6 (4)	19 (7.3)		
Number of solid components, n (%)			0.169	0.681
Single	113 (74.8)	200 (76.6)		
Multiple	38 (25.2)	61 (23.4)		
Solid component distribution, n (%)			1.077	0.299
Concentrated	125 (82.8)	205 (78.5)		
Scattered	26 (17.2)	56 (21.5)		
Solid component location, n (%)			0.117	0.732
Center	83 (55)	148 (56.7)		
Eccentric	68 (45)	113 (43.3)		
Solid component boundary, n (%)			17.573	< 0.001
Unclear	96 (63.6)	110 (42.1)		
Clear	55 (36.4)	151 (57.9)		
Lobe sign, n (%)			40.814	< 0.001
No	136 (90.1)	158 (60.5)		
Yes	15 (9.9)	103 (39.5)		
Vacuole sign, n (%)			0.589	0.443
No	131 (86.8)	233 (89.3)		
Yes	20 (13.2)	28 (10.7)		
Vascular convergence sign, n (%)			4.386	0.036
No	143 (94.7)	231 (88.5)		
Yes	8 (5.3)	30 (11.5)		
Burr sign, n (%)			75.330	< 0.001
No	139 (92.1)	130 (49.8)		
Yes	12 (7.9)	131 (50.2)		
Pleural indentation sign, n (%)			0.012	0.913
No	129 (85.4)	224 (85.8)		
Yes	22 (14.6)	37 (14.2)		
Air bronchogram, n (%)			3.427	0.064
No	137 (90.7)	220 (84.3)		
Yes	14 (9.3)	41 (15.7)		

Table 3. Logistic regression of correlation between imaging features and infiltration degree of lung adenocarcinoma.

Variable	β	SE	Z	OR (95%CI)	P
Mean nodule diameter	0.320	0.049	6.548	1.377 (1.259,1.525)	<0.001
Mean CT value	0.003	0.001	3.378	1.003 (1.001,1.005)	0.001
Solid component ratio	0.050	0.011	4.356	1.051 (1.029,1.076)	<0.001
Lobe sign					
No	0.000			reference	
Yes	2.231	0.405	5.506	9.306 (4.331,21.334)	<0.001
Burr sign					
No	0.000			reference	
Yes	1.454	0.435	3.341	4.280 (1.856,10.332)	0.001

[DOI: 10.61186/ijrr.22.4.909]

Table 4. ROC curve of imaging features for predicting IAC.

Variable	cutoff	AUC	p	Sensitivity	Specificity
Combined	0.607	0.928(0.904, 0.952)	<0.001	0.828(0.782, 0.873)	0.907(0.861, 0.954)
Mean nodule diameter	12.500	0.859(0.823, 0.895)	<0.001	0.736(0.682, 0.789)	0.894(0.845, 0.943)
Solid component ratio	20.969	0.725(0.676, 0.774)	<0.001	0.870(0.829, 0.911)	0.530(0.450, 0.609)
Mean CT value	-473.070	0.659(0.606, 0.712)	<0.001	0.617(0.558, 0.676)	0.728(0.658, 0.799)
Lobe sign	-	0.648(0.610, 0.686)	<0.001	0.395(0.335, 0.454)	0.901(0.853, 0.948)
Burr sign	-	0.711(0.674, 0.749)	<0.001	0.502(0.441, 0.563)	0.921(0.877, 0.964)

Table 5. Clinical data and imaging features of the low-, medium-, and high-risk groups.

Variables	Low-risk group (n = 89)	Medium-risk group (n = 125)	High-risk group (n = 47)	*F/H*	*P*
Gender, n (%)				11.201	0.004
Female	65 (73)	66 (52.8)	23 (48.9)		
Male	24 (27)	59 (47.2)	24 (51.1)		
Age, [y， M(Q1,Q3)]	60.00 (55.00, 68.00)	62.00 (60.00, 67.00)	65.00 (55.50, 67.50)	3.623	0.163
History of smoking, n (%)				5.699	0.058
No	72 (80.9)	114 (91.2)	38 (80.9)		
Yes	17 (19.1)	11 (8.8)	9 (19.1)		
Respiratory symptoms, n (%)				11.390	0.003
No	85 (95.5)	99 (79.2)	39 (83)		
Yes	4 (4.5)	26 (20.8)	8 (17)		
Family history of lung cancer, n (%)				Fisher	0.360
No	84 (94.4)	119 (95.2)	42 (89.4)		
Yes	5 (5.6)	6 (4.8)	5 (10.6)		
CEA, n (%)				Fisher	0.364
Normal	86 (96.6)	117 (93.6)	43 (91.5)		
Increase	3 (3.4)	8 (6.4)	4 (8.5)		
Location of nodule, n (%)				24.366	< 0.001
Inner zone	16 (18)	13 (10.4)	6 (12.8)		
Middle zone	6 (6.7)	36 (28.8)	19 (40.4)		
Outer zone	67 (75.3)	76 (60.8)	22 (46.8)		
Mean nodule diameter,[mm, M (Q1,Q3)]	12.00 (10.00, 15.00)	18.00 (14.00, 22.00)	18.00 (16.00, 21.00)	62.811	< 0.001
Mean CT value, [HU， M(Q1,Q3)]	-559.21 (-643.27, -439.26)	-376.22 (-536.90, -270.18)	-185.97 (-400.67, -140.35)	70.581	< 0.001
Nodule volume, [mm^3,M (Q1,Q3)]	763.04 (582.18, 1499.45)	1998.01 (1120.67, 3383.25)	2242.25 (1909.71, 2374.72)	64.438	< 0.001
Nodule boundary, n (%)				21.712	< 0.001
Unclear	39 (43.8)	24 (19.2)	6 (12.8)		
Clear	50 (56.2)	101 (80.8)	41 (87.2)		
Solid component volume, [mm^3,M (Q1,Q3)]	208.94 (113.07, 468.12)	845.10 (451.28, 1313.22)	512.33 (38.89, 1789.74)	33.185	< 0.001
Solid component ratio(%), M(Q1,Q3)	27.30 (23.49, 29.44)	29.23 (22.60, 63.30)	77.18 (69.54, 82.15)	63.039	< 0.001
Solid component shape, n (%)				Fisher	0.218
Irregular	85 (95.5)	112 (89.6)	45 (95.7)		
Round-like	4 (4.5)	13 (10.4)	2 (4.3)		
Number of solid components, n (%)				3.256	0.196
Single	74 (83.1)	91 (72.8)	35 (74.5)		
Multiple	15 (16.9)	34 (27.2)	12 (25.5)		
Solid component distribution, n (%)				0.147	0.929
Concentrated	71 (79.8)	97 (77.6)	37 (78.7)		
Scattered	18 (20.2)	28 (22.4)	10 (21.3)		
Solid component location, n (%)				10.764	0.005
Center	42 (47.2)	84 (67.2)	22 (46.8)		
Eccentric	47 (52.8)	41 (32.8)	25 (53.2)		
Solid component boundary, n (%)				8.818	0.012
Unclear	48 (53.9)	42 (33.6)	20 (42.6)		
Clear	41 (46.1)	83 (66.4)	27 (57.4)		
Lobe sign, n (%)				1.433	0.488
No	54 (60.7)	79 (63.2)	25 (53.2)		
Yes	35 (39.3)	46 (36.8)	22 (46.8)		
Vacuole sign, n (%)				5.575	0.062
No	85 (95.5)	107 (85.6)	41 (87.2)		
Yes	4 (4.5)	18 (14.4)	6 (12.8)		
Vascular convergence sign, n (%)				5.319	0.070
No	77 (86.5)	116 (92.8)	38 (80.9)		
Yes	12 (13.5)	9 (7.2)	9 (19.1)		
Burr sign, n (%)				10.273	0.006
No	54 (60.7)	61 (48.8)	15 (31.9)		
Yes	35 (39.3)	64 (51.2)	32 (68.1)		
Pleural indentation sign, n (%)				5.263	0.072
No	81 (91)	107 (85.6)	36 (76.6)		
Yes	8 (9)	18 (14.4)	11 (23.4)		
Air bronchogram, n (%)				8.657	0.013
No	83 (93.3)	101 (80.8)	36 (76.6)		
Yes	6 (6.7)	24 (19.2)	11 (23.4)		

[DOI: 10.61186/ijrr.22.4.909]

Table 6. Single-factor logistic regression of low/medium- and high-risk groups.

Variable	β	SE	Z	OR(95%CI)	P
Gender					
Female	0.000			reference	
Male	0.499	0.324	1.541	1.647 (0.872, 3.120)	0.123
Age	0.007	0.019	0.379	1.007 (0.971, 1.046)	0.704
History of smoking					
No	0.000			reference	
Yes	0.453	0.423	1.073	1.573 (0.656, 3.496)	0.283
Respiratory symptoms					
No	0.000			reference	
Yes	0.230	0.435	0.528	1.258 (0.506, 2.843)	0.598
Family history of lung cancer					
No	0.000			reference	
Yes	0.787	0.565	1.392	2.197 (0.664, 6.386)	0.164
CEA					
Normal	0.000			reference	
Increase	0.540	0.608	0.890	1.717 (0.459, 5.290)	0.374
Location of nodule					
Inner zone	0.000			reference	
Middle zone	0.782	0.527	1.485	2.187 (0.813, 6.606)	0.138
Outer zone	-0.296	0.504	-0.588	0.744 (0.291, 2.161)	0.556
Mean nodule diameter	0.070	0.027	2.576	1.073 (1.017, 1.132)	0.010
Mean CT value	0.008	0.001	5.953	1.008 (1.005, 1.011)	<0.001
Nodule volume	0.000	0.000	2.039	1.000 (1.000, 1.000)	0.041
Nodule boundary					
Unclear	0.000			reference	
Clear	1.048	0.462	2.267	2.851 (1.233, 7.779)	0.023
Solid component volume	0.000	0.000	3.223	1.000 (1.000, 1.001)	0.001
Solid component ratio	0.053	0.008	6.533	1.055 (1.039, 1.073)	<0.001
Solid component shape					
Irregular	0.000			reference	
Round-like	-0.664	0.766	-0.867	0.515 (0.080, 1.884)	0.386
Number of solid components					
Single	0.000			reference	
Multiple	0.144	0.372	0.386	1.155 (0.539, 2.342)	0.699
Solid component distribution					
Concentrated	0.000			reference	
Scattered	-0.013	0.393	-0.033	0.987 (0.437, 2.071)	0.974
Solid component location					
Center	0.000			reference	
Eccentric	0.487	0.324	1.504	1.627 (0.863, 3.088)	0.133
Solid component boundary					
Unclear	0.000			reference	
Clear	-0.020	0.326	-0.062	0.980 (0.519, 1.874)	0.950
Lobe sign					
No	0.000			reference	
Yes	0.368	0.325	1.134	1.445 (0.761, 2.731)	0.257
Vacuole sign					
No	0.000			reference	
Yes	0.245	0.492	0.498	1.277 (0.448, 3.176)	0.619
Vascular convergence sign					
No	0.000			reference	
Yes	0.778	0.436	1.783	2.177 (0.888, 4.999)	0.075
Burr sign					
No	0.000			reference	
Yes	0.907	0.342	2.656	2.478 (1.288, 4.956)	0.008
Pleural indentation sign					
No	0.000			reference	
Yes	0.793	0.403	1.967	2.209 (0.972, 4.782)	0.049
Air bronchogram					
No	0.000			reference	
Yes	0.628	0.397	1.583	1.874 (0.833, 3.997)	0.113

CEA:Carcinoembryonic Antigen

[DOI: 10.61186/ijrr.22.4.909]

Table 7. Univariate logistic regression of low/medium- and high-risk groups.

Variable	*β*	*SE*	*Z*	*OR(95%CI)*	*P*
Mean CT value	0.008	0.002	5.062	1.008 (1.005,1.011)	<0.001
Solid component ratio	0.049	0.009	5.472	1.050 (1.033,1.070)	<0.001

Table 8. ROC curve analysis for predicting high-risk group (micropapillary predominant).

Variable	Cutoff	AUC	P	Sensitivity	Specificity
Combined	0.264	0.891(0.844, 0.939)	<0.001	0.745(0.620, 0.869)	0.879(0.835, 0.922)
Mean CT value	-242.920	0.815(0.750, 0.881)	<0.001	0.660(0.524, 0.795)	0.874(0.829, 0.918)
Solid ratio	69.536	0.861(0.810, 0.912)	<0.001	0.766(0.645, 0.887)	0.888(0.846, 0.930)

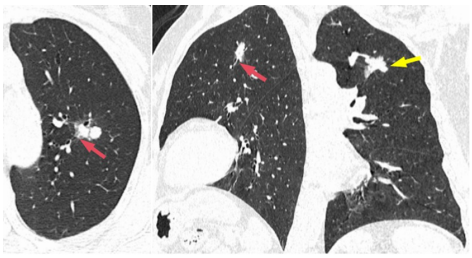

Figure 5. Patient lung CT. Yellow arrows indicate the lobe sign, red arrows indicate the burr sign.

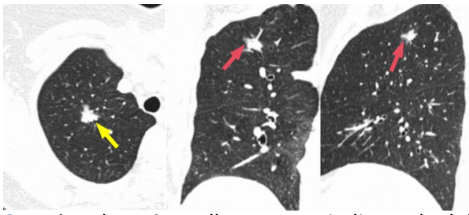

Figure 6. Patient lung CT. Yellow arrows indicate the lobe sign, red arrows indicate the burr sign.

DISCUSSION

The use of low-dose spiral CT in China has led to the detection of an increasing number of pulmonary nodules [10]. A major focus of pulmonary nodule research has always been determining their nature. According to studies, lobe signs, burr signs, and vascular convergence signs are associated with the intensity of pulmonary nodule infiltration. More intense infiltration increases the likelihood of lobe signs, burr signs, and vascular convergence signs [11,12]. In addition, we found that burr signs and air bronchograms differed significantly across pathological types.

This study found that pairwise comparison showed significant differences in burr sign between the high- and medium-risk groups and the high- and low-risk groups. Air bronchogram significantly differed between the low- and medium-risk groups and the high- and low-risk groups, but not the high- and medium-risk groups. These results suggest burr sign may be more common in the high-risk patients, which meets with the study of Miao *et al.* [13]. Air bronchogram may be more common in the medium- and high-risk groups. Reportedly, the proportion of bronchial abnormality increases with the progression of pathological grade in lung adenocarcinoma [14]. This finding is consistent with our study. While the discrepancy in pleural indentation sign among the three pathological subtypes did not reach statistical significance, single-factor regression analysis conducted after consolidating the medium- and low-risk groups indicated that pleural indentation sign may serve as a potential risk factor in the high-risk group. The prevalence of positive pleural indentation sign in the high-risk group exceeded that of the medium- and low-risk groups. While it is not definitive that a higher pathological subtype grade correlates with an increased likelihood of the pleural indentation sign, it may suggest that the sign is more prevalent in individuals at higher risk. Existing research on nodule location and lung cancer infiltration has primarily focused on the lung lobes where the nodules are situated, yielding varied outcomes.

We investigated the correlation between nodule location, infiltration degree, and pathological subtypes through an analysis of the lateral spatial distribution of pulmonary nodules. While there was a significant overall variance in nodule location across pathological subtypes, pairwise comparisons revealed a notable distinction in the low-risk group compared to the other two groups. The limited sample size may account for the inability to clarify the relationship between the horizontal spatial distribution of nodules and pathological subtypes. Therefore, additional comprehensive research is required. It is noteworthy that early lung adenocarcinoma may manifest as pure ground-glass nodules on CT images. As the quantity of tumor cells progressively rises, accompanied by the collapse of alveoli and proliferation of surrounding fibrous tissues, the manifestation of mixed-density ground-glass nodules may occur. The escalation in both size and density of these nodules is indicative of the advancement and aggressiveness of the tumor cells [15]. Although the measurement methods of nodule diameter vary among studies, most studies believe that nodule diameter indirectly reflects its growth characteristics, and a larger nodule corresponds to its higher malignancy. A smaller nodule and the more uniform texture mean it is less likely to be malignant [16,17].

There are literature reports in 432 cases of pulmonary ground-glass nodules, ROC curve analysis revealed at the cutoff of 10.05 mm, IAC can be better distinguished with sensitivity of 88.1% and specificity of 71.9% [18]. These results are consistent with our study. This study showed the average diameter of the IAC group was considerably larger compared with the MIA group. The average diameter can be used as one indicator to assess the properties of pulmonary nodules [19].Computed tomography (CT) values are indicative of nodule density, with smaller numbers of

[DOI: 10.61186/ijrr.22.4.909]

tumor cells initially growing lepidically in the early stages of the disease. As tumor invasiveness progresses, the count of tumor cells gradually rises, leading to alterations in the extracellular matrix and ultimately an increase in lesion density. Research supports a positive correlation between CT values and the degree of tumor invasiveness [20].

In our study, the average CT value of the IAC group was significantly larger.. A meta-analysis by He *et al*. showed the average CT value can well discriminate the invasiveness of ground glass nodules [21]. When the average CT value is ≥ –484 Hu, it is more likely to be IAC, with sensitivity of 78% and specificity of 81%. These results align with the outcomes of our research, indicating that the diagnostic efficacy of pulmonary ground-glass nodules is enhanced by utilizing three-dimensional CT features over two-dimensional layers, total nodule volume over maximum nodule diameter, and solid component volume over maximum diameter of solid components. [22]. Therefore, we incorporated the solid component volume of nodules and the nodule volume in order to assess both the solid component size and the overall size of the nodules. The solid component ratio was determined as the ratio of solid component volume to nodule volume. Given the absence of reliable techniques for precisely measuring the solid components of nodules, many researchers depend on their subjective assessments, leading to a certain degree of reduced accuracy. Zheng et al. found when the CT cutoff was -250 HU, the diagnostic value of identifying solid components in the nodule was the greatest, with AUC of 0.982 [23]. In the medical image processing system used here, the CT cutoff of solid components was set to be -250 HU, and the software automatically calculated the nodule volume and solid component volume. As reported, the ratio of solid components is related to the infiltration degree, and a larger proportion of solid components reflects a higher degree of infiltration [24].

In our study, the solid component ratio in the IAC group was significantly higher. The solid component ratio can be used as an important basis to identify MIA and IAC. This conclusion is basically consistent with most studies. The Japanese JCOG0201 prospective study showed that peripheral non-invasive adenocarcinoma can be accurately predicted using CTR ≤ 25% and diameter ≤ 2 cm [25]. Katsumata et al. found IAC was more likely when the solid proportion was ≥ 50% [26]. Our study shows the nodule is more prone to be IAC when the solid ratio is ≥ 20.96%. The cutoff differs from the other two studies, which may because the solid component ratio used in the other two studies is defined as maximum solid component diameter/maximum nodule diameter in the lung window. We used the solid component volume/nodule volume ratio to analyze pathological subtypes and found that these factors were independently related to higher rates of high-risk lung adenocarcinomas. The average CT value ≥ -242.92 HU and solid component ratio ≥ 69.536% indicated nodules were more likely the high -risk pathological type of lung adenocarcinoma. Zhang et al. pointed out that average CT value ≥ - 472.5 HU and solid component ratio ≥ 27.4% may indicate nonlepidic predominant invasive pulmonary adenocarcinoma in GGNs [27].

Several researchers have examined the relationship between morphology of solid components and pathological subtypes in recent years. The differences between cutoff values may be due to the different groupings. Based on the present study, there is a significant discrepancy in the position of solid components between the three groups. When the low-risk and medium-risk groups are compared pairwise, the solid component position of the high-risk group differs significantly from those of the other two.. The proportions of solid components growing centrally in the high- and low-risk groups were similar (46.8% and 47.2% respectively). The findings indicate that the proportion of solid components growing centrally in the medium risk group was significantly higher at 67.2% compared to the other two groups, implying a higher likelihood of the papillary predominant pathological subtype in cases of invasive adenocarcinoma with centrally growing solid components. This study highlights notable variations in the boundaries of solid components among the three groups. Pairwise analysis indicates a significant distinction in the solid component boundaries between the medium- and low-risk groups, but not in the high-risk group compared to the other two groups. The study does not establish a definitive correlation between the boundaries of solid components and the pathological subtype, suggesting that further extensive research with a larger sample size is warranted.

Pathologically confirmed single pulmonary nodules were included in this retrospective study, which cannot represent all nodules, and some selection bias was present. In light of the increased number of multiple nodules discovered and the development of various imaging analysis systems, this study may be less applicable in the future. Some data rely on human observation, and even with a unified measurement method, there may be certain bias. Moreover, clinical data are less included. In conclusion, despite the presence of limitations, our study conducted a thorough analysis of the associations between imaging features and degree of infiltration with the pathological subtype of ground-glass lung adenocarcinoma, thereby contributing significantly to the clinical assessment of pulmonary nodules.

[DOI: 10.61186/ijrr.22.4.909]

CONCLUSION

CT imaging features can indeed improve the diagnostic efficacy of ground glass nodules and have certain clinical value. Ground glass nodules refer to areas of hazy increased density on CT images, which may represent early lung cancer or other benign lesions. By carefully analyzing the size, shape, density, and other characteristics of these nodules on CT images, doctors can more accurately assess their likelihood of malignancy and make more informed diagnostic decisions. This can help identify potentially malignant nodules early, allowing for timely treatment and improved patient outcomes. Therefore, CT imaging is an important tool in the diagnosis and management of ground glass nodules.

Funding: This study did not receive any funding in any form.

Conflict of interest: The authors have no potential conflicts of interest to report relevant to this article.

Ethical consideration: *Jiangyin Hospital of Traditional Chinese Medicine Medical Ethics number: EC202201*

Author contributions: X.G. and C.H. designed the study and performed the experiments, X.G. collected the data, C.H. analyzed the data, X.G. and C.H. prepared the manuscript. All authors read and approved the final manuscript.

REFERENCES

1. Sung H, Ferlay J and Siegel RL, *et al*. (2021) Global Cancer Statistics 2020: GLOBOCAN Estimates of Incidence and Mortality Worldwide for 36 Cancers in 185 Countries. *Ca-a Cancer Journal for Clinicians*, ***71(3):*** *209-249*.
2. Pizzato M, Li M, Vignat J, *et al*. (2022) The epidemiological landscape of thyroid cancer worldwide: GLOBOCAN estimates for incidence and mortality rates in 2020. *Lancet Diabetes Endocrinol,* ***10 (4):*** *264-272*.
3. Yotsukura M, Asamura H and Motoi N, *et al*. (2021) Long-Term Prognosis of Patients with Resected Adenocarcinoma In Situ and Minimally Invasive Adenocarcinoma of the Lung. *Journal of Thoracic Oncology*, ***16(8):*** *1312-1320*.
4. Watanabe Y, Hattori A and Nojiri S, *et al*. (2022) Clinical impact of a small component of ground-glass opacity in solid-dominant clinical stage IA non-small cell lung cancer. *Journal of Thoracic and Cardiovascular Surgery*, ***163(3):*** *791-801*.
5. Tsao MS, Nicholson AG, Maleszewski JJ, Marx A and Travis WD (2022) Introduction to 2021 WHO Classification of Thoracic Tumors. *Journal of Thoracic Oncology*, ***17(1):*** *e1-e4*.
6. Nicholson AG, Tsao MS and Beasley MB, *et al*. (2022) The 2021 WHO Classification of Lung Tumors: Impact of Advances Since 2015. *Journal of Thoracic Oncology*, ***17(3):*** *362-387*.
7. Moreira AL, Ocampo P and Xia Y, *et al*. (2020) A Grading System for Invasive Pulmonary Adenocarcinoma: A Proposal from the International Association for the Study of Lung Cancer Pathology Committee. *Journal of Thoracic Oncology*, ***15(10):*** *1599-1610*.
8. Choi SH, Jeong JY and Lee SY, *et al*. (2021) Clinical implication of minimal presence of solid or micropapillary subtype in early-stage lung adenocarcinoma. *Thoracic Cancer*, ***12(2):*** *235-244*.
9. Yanagawa N, Shiono S, Abiko M, Katahira M, Osakabe M and Ogata SY (2016) The Clinical Impact of Solid and Micropapillary Patterns in Resected Lung Adenocarcinoma. *Journal of Thoracic Oncology*, ***11 (11):*** *1976-1983*.
10. He J, Li N and Chen WQ, *et al*. (2021) [China guideline for the screening and early detection of lung cancer (2021, Beijing)]. *Zhonghua Zhong Liu Za Zhi*, ***43(3):*** *243-268*.
11. MacMahon H, Naidich DP and Goo JM, *et al*. (2017) Guidelines for Management of Incidental Pulmonary Nodules Detected on CT Images: From the Fleischner Society 2017. *Radiology*, ***284(1):*** *228-243*.
12. Gao F, Sun Y, Zhang G, Zheng X, Li M and Hua Y (2019) CT characterization of different pathological types of subcentimeter pulmonary ground-glass nodular lesions. *British Journal of Radiology*, ***92 (1094):*** *20180204*.
13. Miao Y, Zhang J, Zou J, Zhu Q, Lv T and Song Y (2017) Correlation in histological subtypes with high resolution computed tomography signatures of early stage lung adenocarcinoma. *Translational Lung Cancer Research*, ***6(1):*** *14-22*.
14. Zhang Y, Qiang JW, Shen Y, Ye JD, Zhang J and Zhu L (2016) Using air bronchograms on multi-detector CT to predict the invasiveness of small lung adenocarcinoma. *European Journal of Radiology,* ***85(3):*** *571-577*.
15. Zhang N, Liu JF, Wang YN and Yang L (2020) A nomogram to predict invasiveness in lung adenocarcinoma presenting as ground glass nodule. *Translational Cancer Research,* ***9(3):*** *1660-1669.*
16. Wender R, Fontham ET and Barrera EJ, *et al*. (2013) American Cancer Society lung cancer screening guidelines. *Ca-a Cancer Journal for Clinicians*, ***63(2):*** *107-117*.
17. Qi L, Xue K and Li C, *et al*. (2019) Analysis of CT morphologic features and attenuation for differentiating among transient lesions, atypical adenomatous hyperplasia, adenocarcinoma in situ, minimally invasive and invasive adenocarcinoma presenting as pure ground-glass nodules. *Scientific Reports,* ***9(1):*** *14586.*
18. Fu F, Zhang Y and Wang S, *et al*. (2021) Computed tomography density is not associated with pathological tumor invasion for pure ground-glass nodules. *Journal of Thoracic and Cardiovascular Surgery,* ***162(2):*** *451-459.*
19. Horeweg N, van der Aalst CM and Thunnissen E, *et al*. (2013) Characteristics of lung cancers detected by computer tomography screening in the randomized NELSON trial. *American Journal of Respiratory and Critical Care Medicine*, ***187(8):*** *848-854*.
20. Zhou QJ, Zheng ZC and Zhu YQ, *et al*. (2017) Tumor invasiveness defined by IASLC/ATS/ERS classification of ground-glass nodules can be predicted by quantitative CT parameters. *Journal of Thoracic Disease,* ***9(5):*** *1190-1200.*
21. He S, Chen C and Wang Z, *et al*. (2023) The use of the mean computed-tomography value to predict the invasiveness of ground-glass nodules: A meta-analysis. *Asian Journal of Surgery*, ***46(2):*** *677-682*.
22. Wang H, Yang H, Liu Z, Chen L, Xu X and Zhu Q (2022) [Comparison of Two-dimensional and Three-dimensional Features of Chest CT in the Diagnosis of Invasion of Pulmonary Ground Glass Nodules]. *Zhongguo Fei Ai Za Zhi*, ***25(10):*** *723-729*.
23. Zheng W, Wang Q, Wang Y, Guo F, Wang X and Yu T (2017) [Threshold Segmentation of Pulmonary Subsolid Nodules on CT Images:Detection and Quantification of the Solid Component]. *Zhongguo Fei Ai Za Zhi*, ***20(5):*** *341-345*.
24. Yip R, Li K and Liu L, *et al*. (2018) Controversies on lung cancers manifesting as part-solid nodules. *European Radiology*, ***28(2):*** *747-759*.
25. Suzuki K, Koike T and Asakawa T, *et al*. (2011) A prospective radiological study of thin-section computed tomography to predict pathological noninvasiveness in peripheral clinical IA lung cancer (Japan Clinical Oncology Group 0201). *Journal of Thoracic Oncology*, ***6(4):*** *751-756*.
26. Katsumata S, Aokage K and Nakasone S, *et al*. (2019) Radiologic Criteria in Predicting Pathologic Less Invasive Lung Cancer According to TNM 8th Edition. *Clinical Lung Cancer,* ***20(2):*** *e163-e170.*
27. Zhang P, Li T, Tao X, Jin X and Zhao S (2021) HRCT features between lepidic-predominant type and other pathological subtypes in early-stage invasive pulmonary adenocarcinoma appearing as a ground-glass nodule. *Bmc Cancer,* ***21(1):*** *1124.*

[DOI: 10.61186/ijrr.22.4.909]